Colloids dragged through a polymer solution: Experiment, theory, and simulation

Christof Gutsche,[1] Friedrich Kremer,[1] Matthias Krüger,[2,a)] Markus Rauscher,[2,b)] Rudolf Weeber,[3] and Jens Harting[3]
[1]*Institut für Experimentalphysik I, Universität Leipzig, 04103 Leipzig, Germany*
[2]*Max-Planck-Institut für Metallforschung, Heisenbergstr. 3, 70569 Stuttgart, Germany and Institut für Theoretische und Angewandte Physik, Universität Stuttgart, Pfaffenwaldring 57, 70569 Stuttgart, Germany*
[3]*Institut für Computerphysik, Universität Stuttgart, Pfaffenwaldring 27, 70569 Stuttgart, Germany*

(Received 9 November 2007; accepted 3 July 2008; published online 22 August 2008)

We present microrheological measurements of the drag force on colloids pulled through a solution of λ-DNA (used here as a monodisperse model polymer) with an optical tweezer. The experiments show a drag force that is larger than expected from the Stokes formula and the independently measured viscosity of the DNA solution. We attribute this to the accumulation of DNA in front of the colloid and the reduced DNA density behind the colloid. This hypothesis is corroborated by a simple drift-diffusion model for the DNA molecules, which reproduces the experimental data surprisingly well, as well as by corresponding Brownian dynamics simulations. © *2008 American Institute of Physics*. [DOI: 10.1063/1.2965127]

I. INTRODUCTION

Complex fluids in general and colloid-polymer mixtures in particular are an ideal model system for studying the structure and phase behavior of multicomponent systems. However, they also play a large role in many technological processes such as oil recovery and food science, as well as in most biological systems. For these systems, in addition to the equilibrium properties, the dynamics is important. While for many applications the bulk rheological properties are most relevant, in biological systems, where the size of many constituents is on the microscale, a strong size dependence of the rheological properties has been observed and micron sized probe particles have been used to test the rheology (e.g., by measuring the friction coefficient) on the relevant small length scales, see, e.g., Refs. 1–3.

The friction of probes moving through a solution of macromolecules or of colloids and the diffusion constant of such probe particles are related quantities. The first has been mainly discussed in the context of sedimentation.[4–11] However, the major differences between sedimentation and nanorheology with colloidal probe particles is that in a sedimenting system all particles experience a force (usually gravity) and therefore move, which creates a solvent backflow responsible for a large part of the reduction in the sedimentation velocity as compared to that of a single isolated particle.

The diffusion constant of suspended particles has been discussed in literature extensively,[12–18] and as expected, it is consistently smaller than that in the pure solvent, while the friction constant (as well as the solution's macroscopic viscosity) is always larger than that in the pure solvent.[13,14,18] If one assumes that the Brownian motion is a Markov process, the diffusion constant is coupled to the friction coefficient (the proportionality constant between force and velocity in the linear regime) via the fluctuation-dissipation theorem. Also the latter is directly related to the viscosity via the solution of the Stokes equation. For a large, heavy, and isolated particle suspended in a simple solvent, this is a reasonable approximation,[19,20] but in a suspension of nonvanishing density, the timescale for the dynamics of the surrounding particles and the timescale for the dynamics of the probe particle cannot be separated in general.[18] In addition, structural changes in the solution in the vicinity of the probe particle can enhance[21,22] or reduce[23,24] the friction coefficient. Therefore, one cannot expect a direct relation between the diffusivity of a particle and the macroscopic viscosity of the suspension as it is measured in a viscosimeter. This violation of the Stokes–Einstein relation has been observed experimentally in light scattering experiments[25–27] and by x-ray photon correlation spectroscopy.[28]

In order to elucidate the dynamics of colloids in polymer solutions in more detail, we perform—under well controlled conditions—experiments in which single isolated colloids are held in a stream of λ-DNA solution using optical tweezers. This technique allows us to move a colloid through a highly monodisperse polymer solution at a given velocity (rather than with a given driving force such as in sedimenting systems) and to measure the drag force on the colloid with piconewton resolution at the same time. For high DNA concentrations we find a significantly higher drag force than that predicted by the Stokes equation for the homogeneous solution (which is in apparent contradiction to the observation of an enhanced diffusivity of colloids in similar polymer solutions); however, the force scales approximately linearly with the velocity up to high Peclet numbers. We compare the experimental results to a simplified dynamic density func-

[a)]Present address: Fachbereich Physik, Universität Konstanz, D-78457 Konstanz, Germany.
[b)]Author to whom correspondence should be addressed. Electronic mail: rauscher@mf.mpg.de.

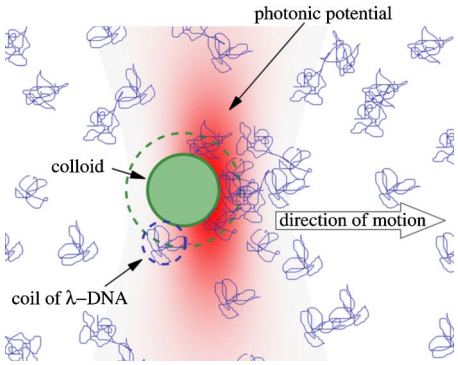

FIG. 1. (Color online) Illustration of the experimental setup. The colloid (green) surrounded by coils of DNA (blue) is held in an optical trap (red). Due to short ranged repulsion, the DNA's center of mass can approach the colloid only up to the green dashed circle.

tional theory for the noninteracting polymers in a flowing solvent and to Brownian dynamics (BD) simulations.

II. EXPERIMENT

A. Materials and methods

Figure 1 illustrates the experimental setup, in which one colloid is held by an optical trap surrounded by a polymer solution of λ-DNA. The DNA stock solution (10 mM tris-HCl, 1 mM ethylenediaminetetraacetic acid (EDTA), 500 μg/ml λ-DNA) was obtained by New England BioLabs (Germany) and diluted to its final concentrations in deionized water. An inverted microscope (Axiovert S 100 TV, Carl Zeiss, Jena, Germany) is used to image the colloid and the optical trap is realized with a diode pumped neodymium doped yttrium aluminum garnet laser (1064 nm, 1 W, LCS-DTL 322; Laser 2000, Wessling, Germany). Its power is stabilized to achieve long-term stability. Additionally, the profile of the laser beam is monitored. After passing an optical isolator, a quarter-wave-plate is used in order to produce circularly polarized light to exclude effects due to reflection differences of the mirrors between the *p* and *s* polarizations of the laser light. The beam is expanded and coupled into the back aperture of the microscope objective (Plan-Neofluor 100×1.30 oil, Carl Zeiss, Jena, Germany). Video imaging and the optical position detection are accomplished by a digital camera (KPF 120, Hitachi, Düsseldorf, Germany). The optical stage is positioned in three dimensions with nanometer resolution using piezoactuators (P-5173CD, Physik Instrumente, Karlsruhe, Germany). The sample cell consists of a closed chamber that can be flushed by a syringe pump with varying solutions. The viscosities are measured with an Ostwald viscosimeter at the same temperature (25 °C room temperature) and with the same λ-DNA solutions as used in the experiment.

B. Data analysis and calibration

The position of the bead in the optical trap is determined by image analysis [Fig. 2(a)].[29,30] For that a sequence of images is recorded (repetition rate of 30 Hz) and analyzed based on the Levenberg–Marquardt algorithm [Fig. 2(b)]. As fit function,

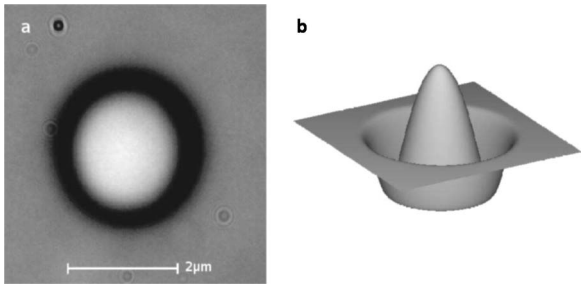

FIG. 2. (a) Microscope image of a single colloid (1.12 μm radius) in the optical trap; (b) fit of the intensity distribution for the image shown in (a) using the Levenberg–Marquardt algorithm.

$$I = I_0 + A(1 - ad)\exp(-d^3), \tag{1}$$

$$d = \left(\frac{x - x_0}{r}\right)^2 + \left(\frac{y - y_0}{r}\right)^2, \tag{2}$$

is used, where (x_0, y_0) is the center position, r is the optical radius, A is the amplitude of the profile relative to the background image intensity I_0, and a is a constant, which is needed in order to consider the dark diffuse ring around the colloid. A variation in r, A, or a in an image sequence indicates the motion in the z direction. The calibration of the optical trap is based on Stokes' law for the pure solvent (here water), as described in detail elsewhere.[31] A typical force constant of the trap is 0.085 pN/nm, corresponding to forces

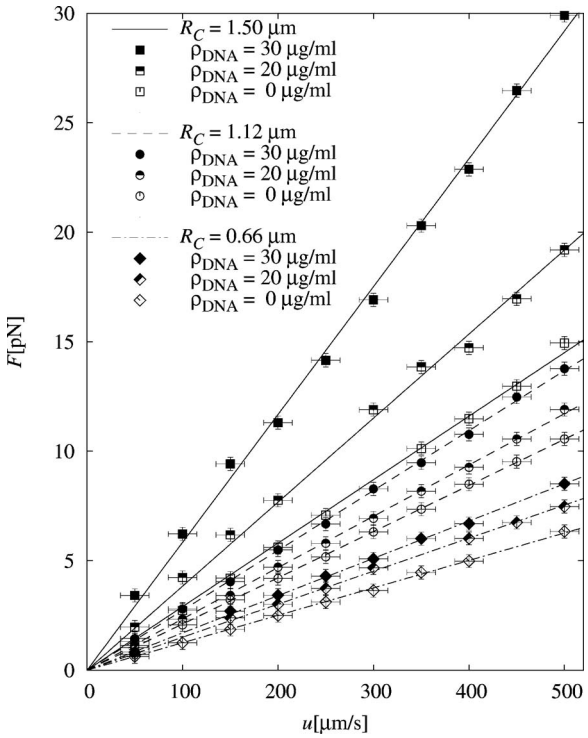

FIG. 3. Drag force F on colloids of radii R_C=1.5 μm (boxes), 1.12 μm (circles), and 0.66 μm (diamonds) in ρ_{DNA}=30 μg/ml (solid symbols) and 20 μg/ml (half-filled symbols), as well as in pure water (open symbols), as a function of the pulling speed u. Also shown are linear fits to the data from which one can extract a density dependent viscosity via the Stokes formula Eq. (3). However, as shown in Fig. 4, these viscosities are inconsistent as they depend on the colloid radius.

TABLE I. Viscosity as a function of DNA concentration extracted from linear fits to the data shown in Fig. 3 using the Stokes formula Eq. (3) compared to the viscosities measured in a viscosimeter. From the viscosimeter data, one obtains an intrinsic viscosity of the DNA of $[\eta]=1.55$. See also Fig. 4.

ρ_{DNA}	0 μg/ml	20 μg/ml	30 μg/ml
$R_C=1.50$ μm	1.03 mPa s	1.36 mPa s	2.07 mPa s
$R_C=1.12$ μm	1.00 mPa s	1.12 mPa s	1.30 mPa s
$R_C=0.66$ μm	1.01 mPa s	1.21 mPa s	1.37 mPa s
Viscosimeter	1.00 mPa s	1.09 mPa s	1.14 mPa s

in the range between 0 and 50 pN, which can be determined with an accuracy of ± 0.15 pN.

In the experiments, no sign of irreversible adsorption of λ-DNA molecules to the colloid is detected. While switching between different flow velocities, the same forces at the same speed are obtained in the range of our uncertainties and after flushing back to pure water, the Stokes force on the colloid could be reproduced.

C. Experimental results

Figure 3 shows the measured force on colloids of sizes $R_C=1.5$, 1.12, and 0.66 μm as a function of the dragging velocity u in pure water as well as for DNA concentrations $\rho_{DNA}=20$ μg/ml and $\rho_{DNA}=30$ μg/ml. Linear fits to the data analyzed in terms of the Stokes drag formula for a colloid of diameter R_C in a DNA solution of viscosity η,

$$F_S^P = 6\pi\eta R_C u, \tag{3}$$

yield the DNA concentration dependent viscosities in Table I (shown in Fig. 4). The viscosities obtained in this manner are significantly larger than the viscosities measured in a viscosimeter for the same DNA solution and they increase with the colloid radius R_C. In other words, the drag forces measured are much larger than the Stokes drag forces computed from the independently measured viscosities. This is a strong indication that on top of the Stokes drag, a second mechanism plays a role.

With the viscosities measured in the viscosimeter we can also extract an effective hydrodynamic radius R_{eff} from a fit of Eq. (3) to the data in Fig. 3. The resulting R_{eff} as a function of ρ_{DNA} are shown in Table II. R_{eff}/R_C increases with ρ_{DNA} but it also varies with R_C: the value for $R_C=1.5$ μm is much larger than the values for the smaller colloids. If the increase in R_{eff} would be due to adsorption of DNA molecules to the colloid, one expects the absolute increase in R_{eff} to a first approximation to be independent of R_C.

TABLE II. Effective colloid radius R_{eff} extracted from the linear fits to the data in Fig. 3.

$\rho_{DNA}=$	0 μg/ml	20 μg/ml	30 μg/ml
$R_C=1.50$ μm	1.50 μm	1.87 μm	2.72 μm
$R_C=1.12$ μm	1.12 μm	1.14 μm	1.27 μm
$R_C=0.66$ μm	0.66 μm	0.73 μm	0.79 μm

The molecular weight of a λ-DNA molecule is $M=31.5\times10^6$ amu$=5.23\times10^{-11}$ μg and its contour length is about 16 μm, leading to a radius of gyration of about $R_g=0.5$ μm. This corresponds roughly to a hydrodynamic radius of $R_H=0.33$ μm ($R_H=0.662R_g$). Based on the hydrodynamic radius and the radius of gyration, we get molecular volumes $V_H=1.5\times10^{-13}$ ml and $V_g=5.2\times10^{-13}$ ml, respectively. For the highest DNA concentrations used in the experiment, i.e., $\rho_{DNA}=50$ μg/ml, this corresponds to volume packing fractions of 14% and 50%, respectively. With this, we can extract the intrinsic viscosity of the DNA solution from the viscosimeter data and get $[\eta]=1.55$. Assuming the intrinsic viscosity for hard-sphere suspensions $[\eta]=\frac{5}{2}$, as predicted in Refs. 32 and 33, we get an effective hydrodynamic radius of $R_\eta=0.28$ μm.

Figure 5 shows the drag force normalized to the pulling velocity u on a colloid of diameter $R_C=1.12$ μm measured as a function of the DNA density ρ_{DNA}. The data point at $\rho_{DNA}=0$ is normalized to the Stokes drag force with the viscosity of water $\eta_w=10^{-3}$ N s/m^2. Clearly, the additional drag due to the presence of the DNA in the solution is not linear in ρ_{DNA} and larger than the drag expected from the

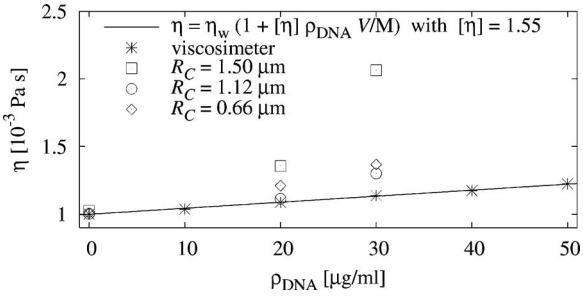

FIG. 4. Viscosity as a function of DNA concentration extracted from linear fits to the data shown in Fig. 3 using the Stokes formula Eq. (3) compared to the viscosities measured in a viscosimeter (see Table I). From the viscosimeter data, one obtains an intrinsic viscosity of the DNA of $[\eta]=1.55$.

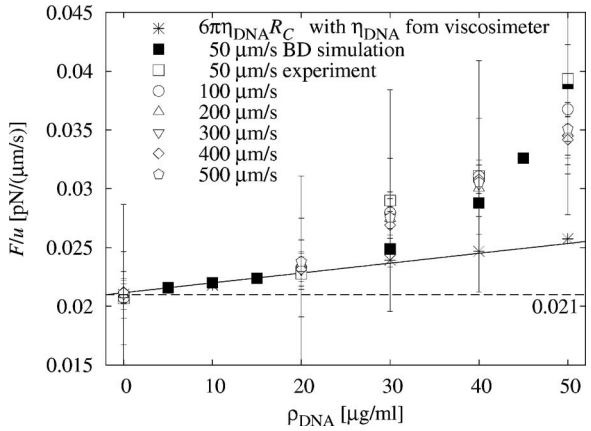

FIG. 5. The measured drag force F on a colloid of radius 1.12 μm normalized to the velocity u as a function of the DNA concentration (open symbols). For the clarity of the presentation only a subset of the experimental data is shown. The data collapse demonstrates that F is proportional to u; however, the dependence on ρ_{dna} is nonlinear. The drag is also significantly larger than expected from the increased viscosity as measured in a viscosimeter (∗). In pure water we obtain $F/u=0.021$ pN/(μm/s) (dashed horizontal line). Also shown are simulation results for polymers with modified mobility (as explained in the text, solid symbols). A fit for concentrations between 0 and 20 μg/ml (solid line) highlights the nonlinearity of the force and the linearity of the viscosity in the density.

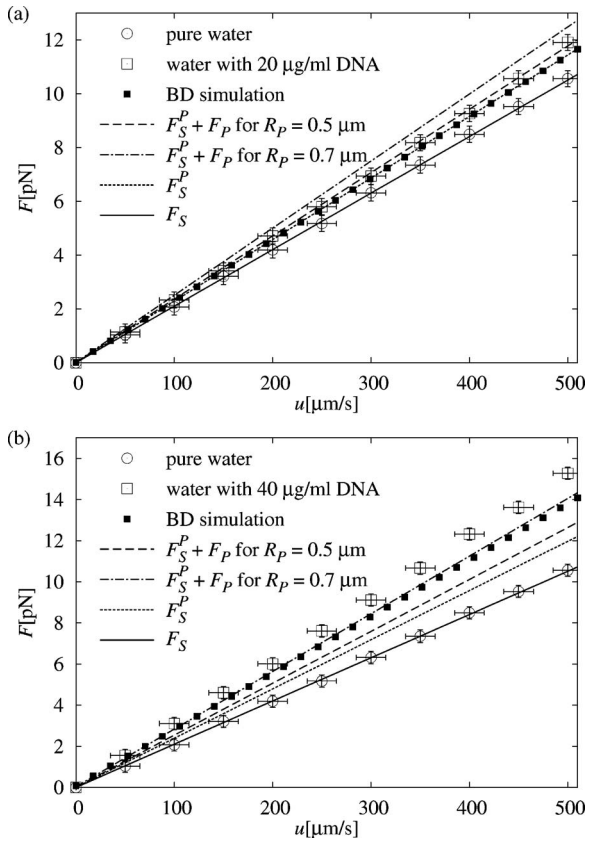

FIG. 6. Drag force F on a colloid of radius 1.12 μm measured in pure water (○) and in a DNA solution (□) as a function of the velocity u. The DNA concentration in (a) is 20 μg/ml and in (b) it is 40 μg/ml. The data are compared to the Stokes friction F_S in pure water (solid line) and in the DNA solution F_S^P (dotted line) calculated from the measured viscosity, as well as to F_S^P plus the contribution F_P from the DNA jammed in front of the colloid for R_P=0.5 μm (dashed line) and for R_P=0.7 μm (dashed-dotted line). Also shown is a fit to BD simulation results between 0 and 50 μm/s (■).

increased viscosity. The error bars for small velocities in Fig. 5 are large due to the uncertainties in determining the velocity u.

In Fig. 6 the measured drag force on the colloid is compared to the calculated Stokes drag force F_S^P in the DNA solution [see Eq. (3)]. The forces are to a good approximation linear in u. The difference between the drag forces for 20 μg/ml DNA and for pure water is only significant for velocities larger than 400 μm/s. For 40 μg/ml DNA we can observe a significant difference already at velocities larger than 100 μm/s. The experimental resolution limits the measurement of the DNA induced drag force to relatively large velocities and to large DNA concentrations. However, Fig. 6(b) clearly shows that the measured drag forces cannot be explained simply by the increased viscosity η_{DNA} of the solution alone.

III. DRIFT-DIFFUSION MODEL

The experimental observation that the drag force on the colloid cannot be explained simply by the increased viscosity in the DNA solution indicates that the dynamics of the DNA in the vicinity of the moving colloid has to be taken into account. The DNA dynamics is governed by the interplay of

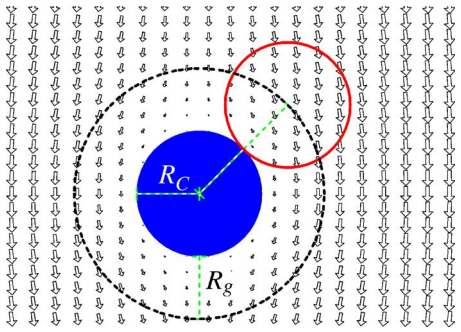

FIG. 7. (Color online) Flow field $\mathbf{v}(\mathbf{r})$ (arrows) around a moving colloid (solid circle) with radius R_C in the frame of reference comoving with the colloid. Particles (e.g., DNA, open circle) with radius R_g can approach the colloid only up to a distance R_C+R_g (dashed circle). The flow field has a component normal to this circle, which leads to an accumulation of particles in front and a depletion of particles in the back of the colloid.

direct intermolecular interactions, hydrodynamics, and the internal degrees of freedom of the DNA coil. It has been shown that an additional drag force due to the rearrangement of solute particles in the vicinity of a dragged colloid can be already obtained in a simple drift-diffusion (DD) model.[21,22] Here we employ the same model to calculate this additional drag force F_P and compare it to the experimental values. Within this model, the DNA molecules are idealized as mutually noninteracting particles having a finite hard core interaction radius with the colloid. The origin of this additional force is illustrated in Fig. 7. Due to the repulsion between the DNA coils and the colloid, the center of mass of the DNA coils can approach the colloid surface only up to a distance of roughly R_g, i.e., the radius of gyration, which creates a forbidden zone for the DNA. The solvent molecules, however, are much smaller and enter this zone, such that the solvent flow field has a component normal to the surface of the forbidden zone pointing inwards in front of the colloid and outwards behind the colloid. DNA coils advected with the solvent will therefore accumulate in front of the colloid and their density will be reduced in its back. This inhomogeneous DNA distribution will lead to an inhomogeneous osmotic pressure and therefore to a force F_P on the colloid.

We will quantify the rearrangement of DNA molecules by calculating the average concentration $C(\mathbf{r})$ (in units of molecules per volume) near the colloid, which in the simple DD model described in Refs. 21 and 22 is given by the stationary solution of the Smoluchowski equation

$$\mathbf{v} \cdot \nabla C = D \Delta C \tag{4}$$

in a frame of reference comoving with the colloid, with the solvent velocity field $\mathbf{v}$ and the DNA (zero concentration) diffusion constant D. In contrast to Ref. 21, $\mathbf{v}(\mathbf{r})$ is not uniform but it is the solution of Stokes' equation for a sphere of radius R_C translating with velocity $\mathbf{u}$ through a resting solvent ($\mathbf{v} \to -\mathbf{u}$ for $|\mathbf{r}| \to \infty$) (see, e.g., Ref. 34 for details),

$$\mathbf{v}(\mathbf{r}) + \mathbf{u} = \frac{3R_C}{4r}\left[\left(1 + \frac{R_C^2}{3r^2}\right)\mathbf{u} + \left(1 - \frac{R_C^2}{r^2}\right)\hat{\mathbf{r}}(\hat{\mathbf{r}} \cdot u)\right], \tag{5}$$

with the unit vector $\hat{\mathbf{r}} = \mathbf{r}/|\mathbf{r}|$. As we model the interaction potential between the colloid and the DNA as a hard-sphere potential, the centers of the DNA coils are excluded from a

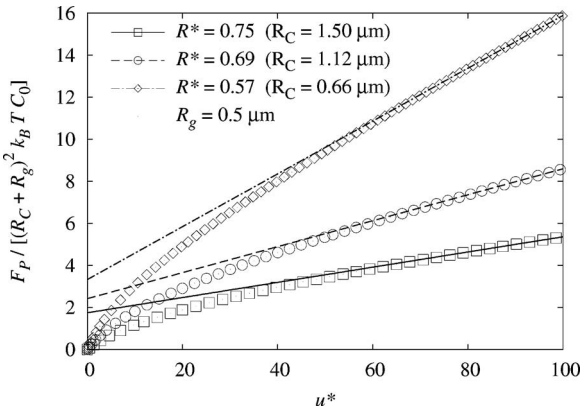

FIG. 8. Numerically calculated drag force for the radii used in the experiment as a function of the Peclet number u^* (symbols) and the affine fits to the data for $80 \leq u^* \leq 100$.

sphere of radius R_C+R_g around the center of the colloid (see Fig. 7). Therefore, the boundary condition for Eq. (4) on this sphere is

$$(\hat{\mathbf{e}}_r \cdot \mathbf{j})|_{r=R_C+R_g} = 0, \tag{6}$$

i.e., the DNA current $\mathbf{j}=\mathbf{v}C-D\nabla C$ normal to the sphere's surface has to vanish. Far from the colloid, the DNA density should be constant, i.e., $C(\mathbf{r}) \to C_0$ for $|\mathbf{r}| \to \infty$. As the mutual interaction between the DNA molecules is neglected, the local pressure $p(\mathbf{r})$ on the colloid surface can be calculated from the ideal gas law $p(\mathbf{r})=k_BTC(\mathbf{r})$. Integrating the local pressure over the surface yields the force F_P on the colloid.

The solution of Eq. (4) depends only on the dimensionless velocity $u^*=u[(R_C+R_g)/D]$ (the Peclet number) of the colloid and the size ratio of the involved particles $R^*=R_C/(R_C+R_g)$. For $R_g/R_C \to 0$, i.e., if the colloid is much larger than the DNA coils ($R^* \to 1$), the surface of the forbidden zone coincides with the colloid surface and the DNA behaves like a solvent molecule. In this limit the solution of Eq. (4) is $C(\mathbf{r})=C_0$, the DNA molecules do not accumulate in front of the colloid, and therefore the additional drag force F_P vanishes.

With a hydrodynamic radius of $R_H=0.33$ μm the Stokes–Einstein relation leads to a diffusion constant $D \approx 6 \times 10^{-13}$ m^2/s. Therefore, the smallest velocities in the experiments ($u=50$ μm/s) correspond to Peclet numbers u^* larger than 100 (depending on the colloid radius). While for small u^* Eq. (4) can be solved analytically in linear order in the Peclet number, we have to use numerical methods for the experimental velocities. To this end, we expand the density field $C(\mathbf{r})$ in spherical harmonics up to order N and obtain a system of $N+1$ ordinary differential equations for the $|\mathbf{r}|$-dependent expansion coefficients, which we solved numerically with AUTO 2000 (Ref. 35) (for details, see Ref. 22). For large u^* a fine numerical discretization (large N) is needed since the thickness of the region in front of the colloid in which the DNA density is enhanced decreases with u^*, while the density in this region increases with u^*. We therefore use $N=100$, which allows us to calculate reliable solutions up to $u^* \approx 100$. For such high velocities the drag force F_P is well approximated by an affine function (see Fig. 8 and also Ref. 21).

TABLE III. Fitting coefficients for the extrapolation of the force F_P to large velocities (Peclet numbers) u^* for the three colloid sizes used in the experiments. The radius of gyration is assumed to be $R_g=0.5$ μm.

R_C (μm)	$R^*=R_C/R_C+R_g$	$\alpha(R^*)$	$\beta(R^*)$
0.66	0.57	3.31	0.126
1.12	0.69	2.43	0.063
1.50	0.75	1.76	0.036

$$F_P(R^*,u^*)/[(R_C+R_g)^2 k_B T C_0] = \alpha(R^*) + \beta(R^*)u^*, \tag{7}$$

which we use to extrapolate to velocities larger than $u^*=100$ (see Fig. 8). The coefficients for fits to the numerical data in the range $80 \leq u^* \leq 100$ for the experimentally relevant values $R_C=1.50, 1.12, 0.66$ μm and $R_g=0.5$ μm are given in Table III. In order to calculate F_P also for other values of R^* and to test the sensitivity of our result to variation in R_g, we use the linear interpolation of the coefficients $\alpha(R^*)$ and $\beta(R^*)$,

$$\alpha(R^*) = 8.146 - 8.427R^*, \tag{8a}$$

$$\beta(R^*) = 0.411 - 0.502R^*. \tag{8b}$$

For the ideal gas law, which we use to calculate the local osmotic pressure on the colloid surface, we need the number density C_0 rather than the mass density ρ_{DNA}, as used in the experiments. With the molecular weight $M=5.23 \times 10^{-11}$ μg we get $C_0(\mathrm{m}^{-3})=1.91 \times 10^{16} \rho_{\mathrm{DNA}}(\mu\mathrm{g/ml})$.

Figure 6 compares the forces on a colloid of size $R_C=1.12$ μm predicted by the DD model to the experimental data. In order to demonstrate the sensitivity of F_P on R_g, we show F_P for the estimated radius of gyration, $R_g=0.5$ μm, as well as for a slightly higher value of $R_g=0.7$ μm. At a concentration of $\rho_{\mathrm{DNA}}=20$ μg/ml [Fig. 6(a)], within the experimental error, the friction of the colloid in the DNA solution can be explained by the increased viscosity in the solution (F_S^P). Nevertheless, theory and experiment are in better correspondence (in particular, for larger velocities) if one takes into account the additional force F_P for a DNA radius of $R_g=0.5$ μm. At a DNA concentration of $\rho_{\mathrm{DNA}}=40$ μg/ml [Fig. 6(b)], the drag force is much larger and it cannot be explained by the increased viscosity only (F_S^P). Taking into account F_P calculated with the DD model still yields a too small drag force (even for $R_g=0.7$ μm). As presented in this section, we calculate F_P in linear order in ρ_{DNA}, i.e., we do not take into account interactions among the DNA molecules. The experimentally measured drag force as a function of the DNA concentration (see Fig. 5) clearly shows a nonlinearity, indicating that these interactions are relevant for concentrations larger than $\rho_{\mathrm{DNA}}=20$ μg/ml. Therefore we performed BD simulations as presented in Sec. IV.

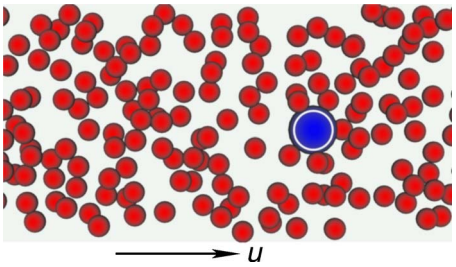

FIG. 9. (Color online) A cut through a part of the simulated system ($28.6 \times 10 \times 1.4$ μm^3). Polymers are shown as small circles and the colloid as a large circle with a ring. The arrow indicates the direction of motion of the colloid. Even though the density map and the density profiles shown in Fig. 10 clearly show an accumulation of polymers in front of the colloid and a depletion region behind it, this cannot be seen from a single snapshot of the system.

IV. BROWNIAN DYNAMICS SIMULATIONS

We simulate the experiments with colloids of radius $R_C = 1.12$ μm using a modified BD method, which, to some extent, includes the hydrodynamics caused by the dragged colloid, as explained in Ref. 22 and summarized below. The polymers and the colloid are modeled as hard spheres with their respective radii. For the polymers we use the radius of gyration $R_g = 0.5$ μm. As the polymers drag along most of the water contained in their volume, the polymers are assigned the mass of water contained in a sphere with radius R_g. The number of polymers in the system is chosen such that the number density (rather than the mass density) of the experiments is reproduced. We use a rectangular simulation volume of $400 \times 40 \times 40$ μm^3 with periodic boundary conditions in all three directions. For a polymer concentration of 40 μg/ml this corresponds to 244 736 polymers. The large system size is necessary due to the long range hydrodynamic interactions caused by the dragged colloid.

The colloid is trapped in a moving parabolic potential $V(r) = \frac{1}{2}ar^2$, mimicking the optical tweezer. The potential has a spring constant of $a = 7.5 \times 10^{-5}$ pN/nm, which gives a better signal to noise ratio than the experimental value of 8.5×10^{-2} pN/nm. Figure 9 shows a snapshot of our simulation setup.

In conventional BD, the two most important aspects of hydrodynamics felt by the suspended particles are taken into account, namely, the Stokes friction and the Brownian motion. Correspondingly, this is done by adding to a molecular dynamics simulation two additional forces. The Langevin equation describes the motion a Brownian particle with radius R at position $\mathbf{r}(t)$ as

$$m\ddot{\mathbf{r}}(t) = 6\pi\eta R\dot{\mathbf{r}}(t) + \mathbf{F}_{\text{rand}}(t) + \mathbf{F}_{\text{ext}}(\mathbf{r},t), \tag{9}$$

where the first term models the Stokes friction in a solvent of viscosity η, $\mathbf{F}_{\text{ext}}(\mathbf{r},t)$ is the sum of all external forces such as gravity, forces exerted by other suspended particles, and, for the colloid, the optical trap. $\mathbf{F}_{\text{rand}}(t)$ describes the thermal noise, which gives rise to the Brownian motion. The random force on different particles, as well as the force on the same particle at different times, is assumed to be uncorrelated. It is further assumed to be Gaussian with zero mean. The mean square deviation of the Gaussian (i.e., the amplitude of the correlator) is given by the fluctuation-dissipation theorem as

$$\langle|\mathbf{F}_{\text{rand}}|^2\rangle = 12\pi\eta R k_B T. \tag{10}$$

This conventional BD scheme is widely used to simulate suspensions (e.g., Refs. 36–38) because it is well understood, not difficult to implement, and needs much less computational resources than a full simulation of the fluid. However, this simulation method does not resolve hydrodynamic interactions between particles. In particular, the long-ranged hydrodynamic interactions between the dragged colloid and the surrounding polymers are not modeled. However, in the system we consider, these interactions are important as the dragged colloid moves quickly and has a strong influence on the flow field around it. Therefore, the BD scheme is modified such that the effect caused by the flow field around the dragged colloid is included. This is achieved by calculating the friction force on the polymers not with respect to a resting fluid ($\mathbf{F} = 6\pi\eta R_c u$) but with respect to the flow field caused by the moving colloid, as given by Eq. (5). The friction force then is

$$\mathbf{F} = 6\pi\eta R_c(\mathbf{u} - \mathbf{v}(\mathbf{r})), \tag{11}$$

where $\mathbf{v}(\mathbf{r})$ is the flow field around the moving colloid at a position $\mathbf{r}$ with respect to the colloid's center. This correction leads to the inclusion of two hydrodynamics-mediated effects. Due to the large component of the flow field along the direction of motion both in front and behind the colloid, polymers are dragged along. Also, as shown in Fig. 7, the flow advects polymers around the moving colloid, i.e., obstacles are moved out of the way to its sides. Both these effects lead to a reduction in drag force on the driven colloid.

In order to reduce computation time, physical quantities are rescaled: the simulation is carried out at a lower temperature. To compensate for this, the viscosity of the fluid as well as all energies are scaled by the same factor. In the present simulations, we scale down the temperature by a factor of 37 500. This scaling leaves the diffusion constant as well as the relative importance of diffusion and motion caused by external forces unchanged. However, it allows for a much larger numerical time step (in this case 60 μs).[39]

From the simulation data, it is possible to measure the effective polymer concentration around the dragged colloid. To accomplish this, we take about 2000 snapshots of the simulation and move each snapshot such that the position of the colloid coincides in each snapshot. We calculate the probability for each of the 200×200 bins to be occupied by a polymer by averaging over all snapshots.

The pictures in Figs. 10(a) and 10(b) depict density maps for a concentration of 10 μg/ml and $u = 40$ μg/ml (in order to obtain a two-dimensional image we take only polymers in a slice 1 μm above and below the colloid center into account). It can be observed that there is a region of high polymer concentration in front and at the sides of the colloid, whereas the region behind the colloid is not yet completely refilled by the polymers. While the accumulation of polymers is stronger at higher concentrations, the depletion region behind the driven colloid is more pronounced at lower concentrations. Figure 10(c) shows the normalized average density of polymers in the direction of motion for concentrations of 10 and 40 μg/ml and $v = 50$ μm/s. In front of the

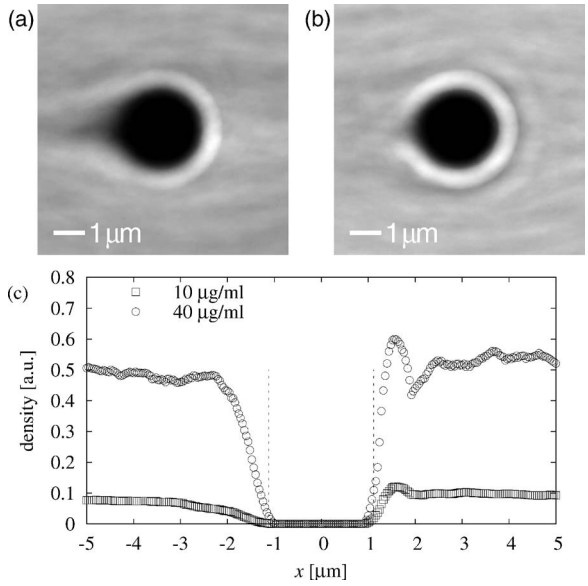

FIG. 10. [(a) and (b)] Polymer density around the colloid averaged over 2000 snapshots of the system at concentrations of 10 and 40 μg/ml, respectively. The dimensions of the snapshots are 8×8 μm^2, averaged over a 2 μm thick slice. Lighter colors denote higher polymer densities. (c) Normalized average polymer density on a line through the colloid center in the direction of motion for concentrations of 10 μg/ml (○) and 40 μg/ml (□) and velocity $u=50$ μm/s. The vertical lines indicate the size of the colloid (±1.12 μm). Polymers accumulate in front of the colloid and the concentration in the back is reduced due to the finite Peclet number of the polymers. While this depletion region is more pronounced at a low polymer concentration [part (a)], the accumulation of polymers is stronger at higher concentrations [part (b)].

colloid, a sharp peak can be observed. For high polymer concentrations, the probability to find a polymer in front of the colloid is close to 1. The region right behind the colloid is almost clear of polymers because the polymers get advected away from the colloid before they can diffuse into this region.

Our model reproduces very well the linear relation between drag force and the drag velocity for different polymer concentrations. As higher drag velocities require a larger system (even with periodic boundary conditions) and short numerical time steps, we are limited to about 80 μm/s by the available computational resources and time. However, the linearity of the drag force with respect to the velocity at sufficiently high velocities allows to extrapolate to the higher velocities used in the experiments. Figure 6 includes a linear fit to the simulation data, which agrees well with the experimental data.

As in the experiments, with Eq. (3) the measured drag force can be interpreted in terms of an effective viscosity. Figure 11 shows the dependency of this viscosity on the velocity for pure water and for polymer concentrations of 20, 40, and 50 μg/ml. Even for a polymer concentration of 50 μg/ml this viscosity is independent of the drag velocity for $u>60$ μm/s, but for lower velocities, we find that the viscosity increases, especially at higher polymer concentrations.

For a fixed drag velocity and varying polymer concentrations, the linear relation between force and concentrations for low polymer concentrations and the stronger nonlinear

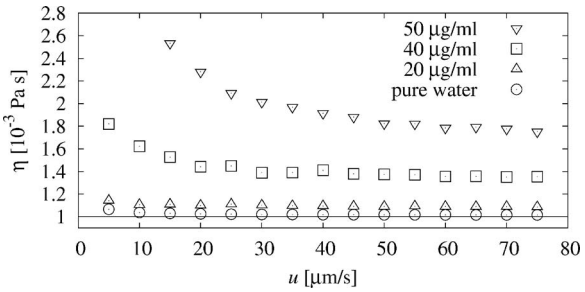

FIG. 11. Effective viscosity [calculated with Eq. (3) from drag force measured in the simulations] vs drag velocity for different polymer concentrations. For velocities larger than about 60 μm/s, the effective viscosity is independent of the velocity even for high polymer concentrations. For low velocities, the drag force increases. The horizontal line indicates the viscosity of the solvent water.

increase for higher concentrations can also be observed, as shown in Fig. 5. It can be seen that there is good quantitative agreement between simulations and experiments.

V. DISCUSSION

The experiments clearly show that the drag force on colloids pulled through a solution of λ-DNA with an optical tweezer cannot be explained by the Stokes force for the viscosity of the solution. It is much higher and increases nonlinearly with the DNA concentration but approximately linearly with the drag velocity. The resolution of the force measurement is ±0.15 pN and, therefore, the difference between the forces on the colloid in the solution and in pure water can be measured only for large concentrations or, in the case of smaller concentrations, only for large velocities. This limits the overlap between the DD theory and the experiments to the lowest concentration of $\rho_{\mathrm{DNA}}=20$ μg/ml used in the experiment.

At this concentration, the volume fraction of the solution taken by the DNA coils (based on $R_g=0.5$ μm) is 0.1 and DNA-DNA interactions can be neglected. The agreement between theory and experiment is very good. For the highest concentration used in the experiments, $\rho_{\mathrm{DNA}}=50$ μg/ml, the volume fraction is 0.5 and DNA-DNA interactions have to be taken into account.

In the BD simulations DNA-DNA interactions have been taken into account. As in the experiments and in the DD theory, the drag force increases linearly with the velocity, at least for large velocities. The nonlinear increase in the drag force with the DNA concentration is also observed in the BD simulations. The hydrodynamic flow field around the colloid (see Fig. 7) is explicitly included in the BD simulation scheme as well as in the DD calculations. It has a component normal to the direction of motion of the colloid, which efficiently reduces the number of DNA molecules accumulated in front of the colloid, while it fills the depletion zone at its back. As demonstrated by the excellent agreement with the experimental data, this hydrodynamic interaction between the colloid and the DNA is the dominant hydrodynamic force in the system. A proper treatment of these forces allows to achieve quantitative accuracy of the simulations.

The agreement between theory and experiment for low concentrations but high velocities is particularly remarkable

considering the simplicity of the models, which neglect many aspects of hydrodynamic interactions or include them in a rather simplistic way (e.g., in terms of an increased viscosity in the DD model). The internal structure of the DNA molecules is neglected in both the DD model and the BD simulations. Apparently, the deformation of the DNA coils in the accumulation region in front of the colloid is not significant. This can be only explained by the proximity of the stagnation point for the solvent flow, which limits the normal component of the solvent velocity field. At this point the shear rate is also smaller than that at the colloid's side, where it goes up to over 700 1/s for $u=500\ \mu\mathrm{m/s}$. With a relaxation time on the order of 0.1 s,[40] this amounts to a Weissenberg number Wi on the order of 70, i.e., much larger than 1. Therefore, the polymer coils should be significantly distorted and viscoelastic effects are to be expected.

In summary, we present a first direct experimental observation of jamming-induced drag enhancement on colloids in polymer solutions. First theoretical approaches to this problem as well as the BD simulations presented in this paper are in good agreement with the experiments and represent a first quantitative modeling of the microrheology of a complex fluid. However, further refinement is needed. Also the apparent contradiction to observations of an enhanced diffusivity of colloids in polymer solutions as compared to the Stokes–Einstein relation based on the viscosity of the bulk polymer solution needs to be addressed. We conjecture that the structure of the polymer solution in the vicinity of the colloid is significantly different for the fast and steady unidirectional motion (with viscosities in the highly nonlinear regime) discussed in this paper and for the slow random motion in diffusion.

ACKNOWLEDGMENTS

F.K., J.H., and M.R. acknowledge support from the Deutsche Forschungsgemeinschaft within the priority program SPP 1164 "Micro- and Nanofluidics." J.H. and R.W. also acknowledge fruitful discussions with M. Hecht. The computations were performed at Forschungszentrum Jülich and at the Scientific Supercomputing Center in Karlsruhe.

[1] F. G. Schmidt, B. Hinner, and E. Sackmann, Phys. Rev. E **61**, 5646 (2000).
[2] M. L. Gardel, M. Valentine, J. C. Crocker, A. R. Bausch, and D. A. Weitz, Phys. Rev. Lett. **91**, 158302 (2003).
[3] J. Liu, M. L. Gardel, K. Kroy, E. Frey, B. D. Hoffman, J. C. Crocker, A. R. Bausch, and D. A. Weitz, Phys. Rev. Lett. **96**, 118104 (2006).
[4] G. K. Batchelor, J. Fluid Mech. **52**, 245 (1972).
[5] G. K. Batchelor, J. Fluid Mech. **119**, 379, (1982).
[6] G. K. Batchelor and C.-S. Wen, J. Fluid Mech. **124**, 495 (1982).
[7] R. Klein and G. Nagele, Nuovo Cimento D **16**, 963 (1994).
[8] H. Hayakawa and K. Ichiki, Phys. Rev. E **51**, R3815 (1995).
[9] J. T. Padding and A. A. Louis, Phys. Rev. Lett. **93**, 220601 (2004).
[10] B. U. Felderhof, Physica A **348**, 16 (2005).
[11] C. P. Royall, J. Dzubiella, M. Schmidt, and A. van Blaaderen, Phys. Rev. Lett. **98**, 188304 (2007).
[12] G. K. Batchelor, J. Fluid Mech. **74**, 1 (1976).
[13] K. F. Freed and M. Muthukumar, J. Chem. Phys. **68**, 2088 (1978).
[14] M. Muthukumar and K. F. Freed, J. Chem. Phys. **70**, 5875 (1979).
[15] G. K. Batchelor, J. Fluid Mech. **131**, 155 (1983).
[16] G. K. Batchelor, J. Fluid Mech. **137**, 467 (1983), CORRIGENDUM.
[17] A. J. Banchio, J. Bergenholtz, and G. Nägele, Phys. Rev. Lett. **82**, 1792 (1999).
[18] J. K. G. Dhont, *An Introduction to Dynamics of Colloids*, Studies in Interface Science, Vol. II (Elsevier, Amsterdam, 1997).
[19] D. Bedeaux and P. Mazur, Phys. Lett. **43A**, 401 (1973).
[20] D. Bedeaux and P. Mazur, Physica A **80**, 189 (1975).
[21] T. M. Squires and J. F. Brady, Phys. Fluids **17**, 073101 (2005).
[22] M. Rauscher, M. Krüger, A. Dominguez, and F. Penna, J. Chem. Phys. **127**, 244906 (2007).
[23] R. Tuinier and T. Taniguchi, J. Phys.: Condens. Matter **17**, L9 (2005).
[24] R. Tuinier, J. K. G. Dhont, and T.-H. Fan, Europhys. Lett. **75**, 929 (2006).
[25] G. S. Ullmann, K. Ullmann, R. M. Lindner, and G. D. J. Phillies, J. Phys. Chem. **89**, 692 (1985).
[26] G. D. J. Phillies, G. S. Ullmann, K. Ullmann, and T.-H. Lin, J. Chem. Phys. **82**, 5242 (1985).
[27] G. D. J. Phillies, C. Malone, K. Ullmann, G. S. Ullmann, J. Rollings, and L.-P. Yu, Macromolecules **20**, 2280 (1987).
[28] A. Tuteja, M. E. Mackay, S. Narayanan, S. Asokan, and M. S. Wong, Nano Lett. **7**, 1276 (2007).
[29] B. Ovryn and S. H. Izen, J. Opt. Soc. Am. A **17**, 1202 (2000).
[30] B. Ovryn, Exp. Fluids **29**, S175 (2000).
[31] K. Svoboda and S. M. Block, Annu. Rev. Biophys. Biomol. Struct. **23**, 247 (1994).
[32] A. Einstein, Ann. Phys. **34**, 591 (1911).
[33] T. F. Ford, J. Phys. Chem. **64**, 1168 (1960).
[34] L. D. Landau and E. M. Lifshitz, *Fluid Mechanics*, Course of Theoretical Physics, Vol. 6, 2nd ed. (Elsevier Butterworth-Heinemann, Amsterdam, Boston, Heidelberg, 2005).
[35] See http://sourceforge.net/projects/auto2000/ for more information on AUTO 2000.
[36] C. Reichhardt and C. J. Olson Reichhardt, Phys. Rev. Lett. **96**, 028301 (2006).
[37] C. Reichhardt and C. J. Olson Reichhardt, Phys. Rev. E **69**, 041405 (2004).
[38] C. Reichhardt and C. J. Olson Reichhardt, Phys. Rev. Lett. **92**, 108301 (2004).
[39] M. Hecht, J. Harting, T. Ihle, and H. J. Herrmann, Phys. Rev. E **72**, 011408 (2005).
[40] L. Fang, H. Hu, and R. G. Larson, J. Rheol. **49**, 127 (2005).